PCCP

Accepted Manuscript

ROYAL SOCIETY OF CHEMISTRY

www.rsc.org/pccp

Energy & Environmental Science

ARTICLE

Zeolites for the selective adsorption of sulfur hexafluoride

I. Matito-Martos[a], J. Álvarez-Ossorio[a], J.J. Gutiérrez-Sevillano[a], M. Doblaré[b], A. Martin-Calvo*[a], and S. Calero*[a]

Received 00th January 20xx,
Accepted 00th January 20xx

DOI: 10.1039/x0xx00000x

www.rsc.org/

Molecular simulations have been used to investigate at molecular level the suitability of zeolites with different topology on the adsorption, diffusion and separation of a nitrogen-sulfur hexafluoride mixture containing the latter at low concentration. This mixture represents the best alternative for the sulfur hexafluoride in industry since it reduces the use of this powerful greenhouse gas. A variety of zeolites are tested with the aim to identify the best structure for the recycling of sulfur hexafluoride in order to avoid its emission to the atmosphere and to overcome the experimental difficulties of its handling. Even though all zeolites show preferential adsorption of sulfur hexafluoride, we identified local structural features that reduce the affinity for sulfur hexafluoride in zeolites such as MOR and EON, providing exclusive adsorption sites for nitrogen. Structures such as ASV and FER were initially considered as good candidates based on their adsorption features. However, they were further discarded based on their diffusion properties. Regarding operation conditions for separation, the range of pressure that spans from $3{\cdot}10^2$ to $3{\cdot}10^3$ kPa was identified as the optimal to obtain the highest adsorption loading and the largest SF_6/N_2 selectivity. Based on these findings, zeolites BEC, ITR, IWW, and SFG were selected as the most promising materials for this particular separation.

Introduction

Sulfur hexafluoride (SF_6) is an inorganic, colorless, odorless, nonflammable, and nontoxic gas with an octahedral structure in which a central sulfur atom is surrounded by six fluorine atoms. Besides its low toxicity, this gas also exhibits a high dielectric strength, arc-quenching properties, and high thermal and chemical stability. It is mainly used in the electrical industry as insulating gas for transmission and distribution of electrical energy[1, 2]. Sulfur hexafluoride is also used in aluminum and magnesium foundries, semiconductor manufacturing, inert solvent for supercritical fluid chemical reactions, and for medical applications such as ophthalmologic surgeries as inert gas[3] and as contrast agent for ultrasound imaging to examine the vascularity of tumors[4]. As a result of its different uses, the global concentration of this gas has increased from less than 1 ppt in 1975 to about 7-8 ppt nowadays[5, 6]. From the environmental point of view sulfur hexafluoride is an efficient infrared absorber and a potent greenhouse gas with a global warming power about 23,900 times larger than this of CO_2[7, 8]. Even with low concentration of SF_6 in the atmosphere the overall contribution to global warming is estimated to be about 0.2 %, as a result of its high chemical stability and the fact that its atmospheric degradation is very slow. Sulfur hexafluoride is inert in the troposphere and the stratosphere and has an estimated atmospheric lifetime of 800–3200 years[9]. Therefore its contribution to global warming is expected to be cumulative and quasi-permanent. The worldwide goal is to reduce the absolute amount of sulfur hexafluoride as a consequence of its long-term effects on the environment. This gas was included in the Kyoto Protocol, which goal is to contain global emissions of the main anthropogenic gases. Additionally, in Europe, sulfur hexafluoride falls under the F-Gas directive which bans or controls its use for several applications. Hence, efficient methods are under development for handling and recovering sulfur hexafluoride after industrial usage, or to find an alternative gas for insulation of electrical equipment.

Among the methods for the treatment of sulfur hexafluoride, decomposition by plasma, electrical discharge, or spark are quite efficient methods but many undesirable wastes are produced as well[10, 11]. Some techniques based on catalytic decomposition are able to achieve ratios of decomposition similar to the formers but with fewer wastes[5, 12, 13]. Sulfur hexafluoride is also easy to recover due to its relative high boiling point[14] (204.9 K at atmospheric pressure) that makes possible an effective liquefaction. However, for mixtures containing nitrogen and low concentration of SF_6 the compression pressure needed for its recovery raises from 2 MPa at room temperature to 20 MPa for contents lower than 10% of SF_6 in the mixture[15]. This makes difficult the application of liquefaction procedures[16-18] though this is an interesting mixture as supposes a way to reduce the amount of SF_6 used while keeping all its properties[14]. As an alternative recovery

[a] Department of Physical, Chemical and Natural Systems, University Pablo de Olavide, Sevilla 41013, Spain
[b] Abengoa Research, Abengoa, Campus Palmas Altas, Energía Solar, 1. (Palmas Altas) 41014 Seville, Spain
† Electronic Supplementary Information (ESI) available: See
DOI: 10.1039/x0xx00000x

method or as a way to increase the concentration of SF_6 in mixtures, adsorption in porous materials is an interesting option. The general idea is to capture the molecules of sulfur hexafluoride and exhaust the other component, nitrogen in this case, to the atmosphere using porous materials as molecular sieves.

There are some studies in the literature that report experimental and theoretical adsorption of sulfur hexafluoride in different porous materials such as zeolites[15, 19, 20], metal organic frameworks[21-23], carbon nanotubes[24, 25], or pillared clays[26, 27]. Besides, zeolites have been proved to be good candidates as molecular sieves[28, 29]. These materials exhibit a large variety of pore sizes and shapes as well as other interesting properties[30-32] (i.e. ordered structure, high surface area or thermal stability) to capture, separate or to purify mixtures containing small gases[33, 34]. Zeolites are aluminosilicates consisting of tetrahedral units with four oxygen atoms bonded to a central atom (T) that can be silicon, aluminum, or other four-fold coordinated metal. The tetrahedral basic units are connected via oxygen atoms, generating 3D structures with cages and/or channels giving a huge variety of possibilities difficult to screen experimentally. Additionally, the strong restriction over the uses of SF_6 hinders even more their handling making a challenge to identify the most adequate material for the processes of interest (separation and/or capture).

We analyze the suitability of 41 zeolites for the adsorption of sulphur hexafluoride and its separation from a mixture containing nitrogen. This study is carried out using molecular simulations that overcome the serious limitations faced by experimentalists when dealing with this specific gas. As an additional contribution, we provide a reliable model for sulphur hexafluoride that reproduces the properties of this gas in the bulk as well as the few experimental studies on its adsorption in zeolites. The combination of geometric criteria with adsorption properties, structural features, and diffusion of the molecules inside the pores is an important strength of this work, offering consistent identification of the optimal structures as well as information about the most efficient operation conditions for this particular separation. The knowledge gained here will enable the scientific and industrial community to set the bases for the identification, design, and synthesis of structures with optimal performance on the separation of this particular –and difficult to handle- type of mixtures

The information given in this paper is organized as follows. In section 2 we describe the models for adsorbates and adsorbents, as well as the simulation techniques. In section 3 we discuss the results obtained from the force field parameterization of sulfur hexafluoride as well as the adsorption and diffusion obtained for the two molecules in each zeolite. Finally, in section 4 we summarize some concluding remarks.

Methodology

Van der Waals interactions were described by 12-6 Lennard-Jones potential using a cutoff distance of 12 Å, where the interactions were truncated and shifted without tail corrections. Electrostatic interactions were considered by using Coulombic potentials and Ewald summations with a cutoff distance of 12 Å. These simulation conditions are commonly used to study the adsorption in confined systems[29, 33, 35]. For the molecule of nitrogen, we used a previous rigid model developed by Martin-Calvo *et al.*[36]. The symmetric structure of sulfur hexafluoride is also rigid with a bond length of 1.565 Å between the central sulfur atom and the fluorine atoms, while no charges were used. Lennard-Jones parameters for sulfur hexafluoride were obtained by fitting to the experimental Vapor–Liquid Equilibrium (VLE) curve[37]. Adsorbate-adsorbate van der Waals interactions are taken into account by Lorentz–Berthelot mixing rules[38].

We selected 41 zeolites with different geometry and topology from the International Zeolite Association (IZA)[39], considering the frameworks as rigid. The effect of zeolite flexibility in adsorption is usually small but it could play a role on the diffusivities. However, one should be cautious before using flexibility since diffusion values when flexibility is included strongly depend on the model used[40]. On the other hand we are not focusing here on the quantitative values for diffusivities but on the removal of these zeolites in which the diffusion of sulfur hexafluoride is not fast enough. This selection is based not only in Molecular Dynamics simulations but also in the information of the pore limiting diameter provide by the IZA Structure Commission. In absence of experimental data for comparison we are of the opinion that the use of rigid models in zeolites that are not suffering structural changes could lead to more reliable conclusions than the use of flexible models.

Adsorbate-adsorbent interactions were defined by these of the oxygen atoms of the framework (Ozeo) with the atoms of the adsorbed molecules. We used newly reported parameters to reproduce the interactions between the molecules of nitrogen and zeolites[41], while we provide parameters for sulfur hexafluoride. The set of charges of the frameworks was taken from Garcia-Sanchez *et al.*[42]. Details of the interaction parameters and models used are compiled in Table 1.

The selected structures were classified according to their channel system dimensionality (1-3 dimensional) and the ratio of the maximum diameter of a sphere that can be included and diffuse inside the zeolite[39]. Taking into account this ratio, each material was classified as either channel or interconnected cage system, where an interconnected caged system is recognized by ratios up to 1.5, and channels system otherwise. We selected structures within each of these six classes to obtain representative sets: 1D channels (ASV, DON, CFI, ITW, JRY, LAU, LTL, MOR, PON), 2D channels (AFR, EON, FER, IWV, NES, SFO, SFG, TER), 3D channels (AFY, BEC, BOG,

Table 1 Lennard-Jones parameters and partial charges of the adsorbates and the adsorbents

Atom 1	Atom 2	ε/k_B (K)	σ (Å)	Charge (e⁻)
Adsorbed Molecules				
$F(SF_6)$	$F(SF_6)$	73.130	2.843	-
$S(SF_6)$	$S(SF_6)$	-	-	-
$N(N_2)$	$N(N_2)$	38.298	3.306	-0.405
$Site(N_2)$	-	-	-	0.810
Zeolite				
O(zeo)	O(zeo)	-	-	-0.393
Si(zeo)	Si(zeo)	-	-	0.786
Adsorbed Molecules - Zeolite				
$F(SF_6)$	O(zeo)	80.304	2.962	-
$S(SF_6)$	O(zeo)	-	-	-
$N(N_2)$	O(zeo)	60.580	3.261	-
$Site(N_2)$	O(zeo)	-	-	-

MEL, MFI, ITR, SBT, STW), 1D interconnected cages (ITE, MTF, SAS), 2D interconnected cages (DDR, LEV, MWW), 3D interconnected cages (CHA, EMT, ERI, FAU, LTA, KFI, OBW, PAU, RHO, SBE). Fig. 1 shows the energy grid surface of representative structures of each group. Some characteristics of the zeolites, such as their unit cell lengths, pore volume, and surface area can be found in **Table S1** in the Electronic Supporting Information (ESI).

Simulations were performed using RASPA[43]. We carried out Gibbs-ensemble Monte Carlo simulations[44] to compute the VLE curve of sulfur hexafluoride. During the simulations, the parameters were fitted to reproduce the experimental curve[37]. This is the first and the most important step for the performance of adsorption studies in porous systems[35, 42]. Monte Carlo simulations in the Canonical ensemble (CMC) were performed to compute isosteric heats of adsorption using the Widom test particle method[44]. These simulations were carried out in the limit of zero loading with only one molecule in the system and provide energies and entropies of adsorption at low loading. Adsorption isotherms were computed using Monte Carlo simulations in the Grand Canonical ensemble (GCMC), with fixed temperature, volume, and chemical potential. Chemical potential is associated to fugacity, and fugacity is directly related to pressure by the fugacity coefficient through the Peng-Robinson equation of state. Based on the type of gas and operating conditions, pressure can be equate to fugacity (fugacity coefficient = 1). To compare simulated and experimental adsorption isotherms, absolute adsorption has been converted to excess adsorption[39, 45]. To study diffusion properties of sulfur hexafluoride in the structures, self-diffusion in each zeolite was calculated through the slope of the Mean Square Displacements (MSD), obtained by Molecular Dynamics (MD) simulations in the canonical ensemble. MD simulations started from equilibrium conditions with two molecules in the system previously achieved using a short CMC simulation.

In the MD, successive configurations of the system were generated by integrating Newton's laws of motion using the velocity-Verlet's algorithm. Nosé–Hoover thermostat was used with a time scale on which the system thermostat evolves of 0.15 ps. Simulations run for 45,000 ps using an integration time step of $t = 5 \times 10^{-4}$ ps.

Sodalites and other cavities that are inaccessible from the main channel need to be blocked[46, 47]. To identify inaccessible cavities we use Monte Carlo simulations and Molecular Dynamics. The first method identifies energetic preferential adsorption sites and the second informs about the diffusion of these molecules. The sites on each structure from which the molecules were unable to scape after 0.15 ns were properly blocked. Blocking can be achieved by placing additional hard-sphere particles inside the pockets that prevent adsorbates from accessing these pockets, or just using a list of geometric volume shape/sizes (e.g. spheres using an appropriate radius) that are automatically considered an overlap in Monte Carlo, either computed in advance or on-the-fly[48]. In RASPA, the blocking is implemented using a list of geometric descriptions of the inaccessible volumes.

Some other properties of the structures such as surface area and pore volume were further computed for later analysis. Additional information about these methods can be found elsewhere[44].

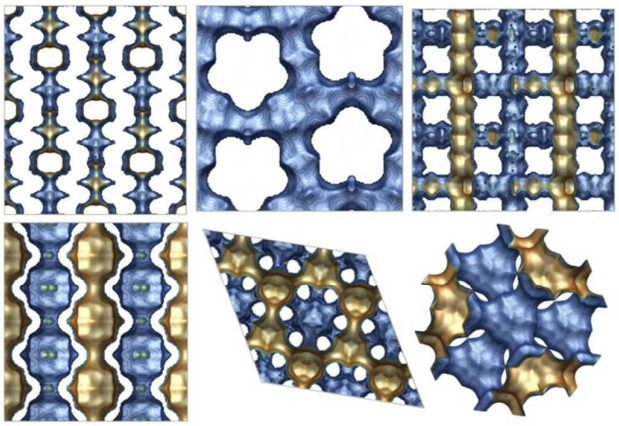

Fig. 1 Energy grid surface of representative zeolites. Channels (top): 1D, 2D, and 3D – MOR, SFG, and MFI, respectively; interconnected cages (bottom): 1D, 2D, and 3D – SAS, DDR, and FAU, respectively. The accessible surface is colored in brown while the inaccessible surface is depicted in blue.

Results and discussion

To reproduce the experimental VLE curve of a given molecules is of capital importance in adsorption studies[49]. As a first approach we compute this curve using the force field parameters of sulfur hexafluoride proposed by Pawley *et al.*[50], Pradip and Yashonath[51], and Dellis and Samios[52]. The critical parameters were predicted for all the models using the density scaling law and the law of rectilinear diameters[53-56] and compiled in Table 2. We compare the results obtained using these three set of parameters with experimental data from the National Institute of Standards and Technology[37] (NIST). This comparison is shown in Fig. 2. The first two models provide similar curves and good agreement with the experiments at up

Table 2 Critical parameters calculated for Sulfur Hexafluoride.

	T_c (K)	D_c (kg m^{-3})	P_c (MPa)
Experimental[37]	318.730	743.810	3.755
This Work	314.830	743.541	3.529
Pawley *et al.*[50]	284.210	765.149	3.712
Pradid and Yashomat[51]	282.890	816.992	3.448
Dellis and Samios[52]	299.975	766.534	4.033

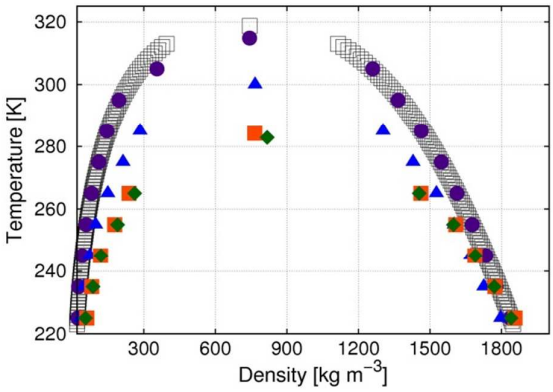

Fig. 2 Vapor-liquid equilibrium curve of sulfur hexafluoride. Comparison of experiments[37] (empty squares) with the simulation values obtained using the force field parameters proposed by Dellis and Samios[52] (blue triangles), Pradid and Yashomat[51] (green diamonds), Pawley *et al.*[50] (orange squares), and the new set of parameters (purple circles).

to 240 K. However, the curves obtained by simulation using these models deviate at higher temperatures, both in the liquid and in the vapor branches. The VLE curve obtained using the parameters proposed by Dellis and Samios[52] shows better agreement with the experiment in the vapor branch, but only for temperature below 260 K. The agreement with experiments in the liquid branch is also reasonable up to this point. The three previous models highly underestimate the critical temperature (5%-11%) and overestimate the critical density (3%-10%). Taking into account these results, we refitted the parameters given by Dellis and Samios[52] to reproduce the experimental curve and the critical parameters, obtaining a new set that is listed in Table 1. The values obtained with the new set of parameters are depicted with circles in Fig. 2 and compiled in Table 2.

The parameters that we have developed to describe adsorbate-adsorbent interactions are also included in Table 1. These parameters were developed by fitting to the experimental adsorption isotherm of sulfur hexafluoride in MFI zeolite at 308 K and further validated for a range of temperature that spans from 277 K to 353 K. It should be mentioned that available experimental data of sulfur hexafluoride adsorption in nanoporous materials is rather scarce due to the difficulties of handling. Simulated and experimental adsorption isotherms of sulfur hexafluoride in MFI are shown in Fig. 3. The figure shows the excellent agreement obtained for the calculated sulfur hexafluoride adsorption isotherms in MFI (277 K, 308 K, and 353 K) and available experimental data from Dunne *et al.*[57] (304.94 K) and from Sun *et al.*[58] (276.95 K, 307.95 K, and 352.75 K).

To validate the adsorbate-adsorbent interaction parameters, isosteric heat of adsorption (Q_{st}) in the limit of zero coverage in MFI was computed at 305 K and compared with the experimental values from Cao and Sircar[20], Dunne *et al.*[57], and MacDougall *et al.*[59] . The calculated heat of adsorption (34.47 kJ/mol) is in very good agreement with this obtained by Dunne *et al.*[57] (34.40 kJ/mol) and slightly overestimates the value given by MacDougall *et al.*[59] (33.05 kJ/mol). Larger discrepancies are found with the heat of adsorption reported by Cao and Sircar[20] (above 39 kJ/mol).These discrepancies can be attributed to the fact that the formers works measured the heats of adsorption for crystal samples whereas the latter used samples with binders.

The isosteric heats of adsorption of nitrogen and sulfur hexafluoride were computed for all zeolites to evaluate the strength on the interaction of the two molecules with the structures. Direct comparison (shown in Fig. 4) can be used as a rough estimation of the affinity of the different zeolites for one component over the other. As expected from the difference in size of the two molecules (the kinetic diameters of SF_6 and N_2 are 5.128 Å, and 3.64-3.80 Å, respectively), the heat of adsorption obtained for sulfur hexafluoride in all zeolites is higher in absolute number than the obtained for nitrogen. The energy due to the size of the molecule predominates over Columbic energy considering that we use a non-charged model for sulfur hexafluoride, while nitrogen has a molecular quadrupole moment of 1.17 D Å[36] (reproducing the experimental value). Only ITW and JRY do not follow the general trend exhibiting lower values of heat of adsorption for sulfur hexafluoride than for nitrogen. This is not depicted in the figure because the ratio between heats of adsorption is lower than 1. The low values of heat of adsorption for sulfur hexafluoride in ITW (-4.43 kJ/mol) and JRY (-10.02 kJ/mol) zeolites indicate that sulfur hexafluoride is not adsorbed in these zeolites. Therefore, since the aim of this paper is to find structures for the selective capture of sulfur hexafluoride we discard these two structures from further analysis.

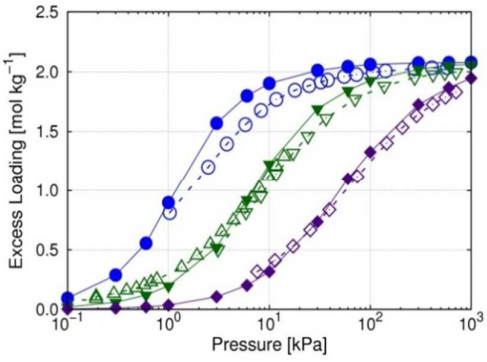

Fig. 3 Comparison of simulated (closed symbols) and experimental (open symbols) adsorption isotherms of sulfur hexafluoride in MFI at 277 K (blue circles), 308 K (green down triangles), and 353 K (purple diamond) from Sun et al.[58]; and at 304.94 (green up triangles) from Dunne *et al.*[57].

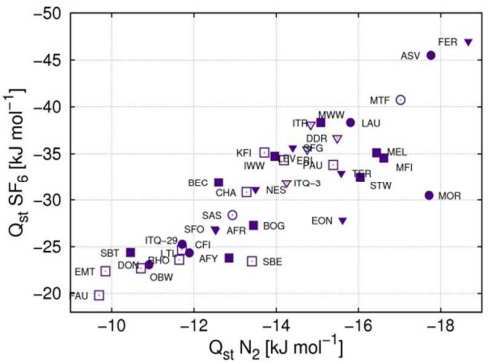

Fig. 4 Isosteric heats of adsorption of sulfur hexafluoride and nitrogen in a variety of zeolites at 298 K. Open symbols show the results obtained for channel-type zeolites and closed symbol for the interconnected-type zeolites. The directionally of the pore space is represented by circles (1D), down triangles (2D), and squares (3D).

ASV and FER show the highest heat of adsorption for both sulfur hexafluoride (above -45 kJ/mol) and nitrogen (about -18 kJ/mol), affecting to the selective adsorption. On the other hand, in EON, MOR and SBE the ratio between heats of adsorption (SF_6/N_2) seems to be the lowest. The heats of adsorption of sulfur hexafluoride and nitrogen as a function of the pore volume of the zeolites are depicted in Fig. S1 and S2 in the ESI. As a general rule we find that the lower the pore volume of the zeolites the highest the heat of adsorption, both for sulfur hexafluoride and nitrogen.

For a better understanding of the adsorption selectivity at low loading, the ratio between the heats of adsorption of both gases (sulfur hexafluoride over nitrogen) as a function of the pore volume of each zeolite is also depicted in Fig. 5. This figure confirms that AFY, EON, MOR and SBE are the worst candidates for the separation if we base the analysis only on the adsorption properties at low loading. The strength of the interaction SF_6-zeolite is less than twice the interaction N_2-zeolite in these four zeolites since some local structure features dominate the adsorption behavior[60]. To seed light to this behavior we computed average occupation profiles of the gases inside the pores of the zeolites (Fig. S3-4 and S5-6 in the ESI).

Zeolite MOR consists of parallel channels with small side-pockets that are preferential sites of adsorption for small molecules such as CO_2, CO or N_2[29]. The average occupation profile (Fig. S3 in the ESI) reveals that the molecules of nitrogen tend to adsorb preferentially in these pockets while sulfur hexafluoride is only adsorbed in the main straight channels as the size of the gate ring prevents them to enter the pockets (limiting diameter 3.4*x*4.8 Å)[39]. The confinement of the molecules of nitrogen in the side-pockets explains the large values obtained for the heat of adsorption in comparison with these of sulfur hexafluoride (adsorbed in the big main channels). This explanation could be extended to EON too since this structure also has side-pockets where only nitrogen is able to enter, while sulfur hexafluoride is adsorbed in the main channels (Fig. S4 in the ESI). Additionally, in this structure, triangular cages connecting side-pockets are found, but are not accessible for molecules with diameter larger than 3.6 Å, excluding therefore both molecules (Fig. S5 in the ESI). In SBE the main channels where the molecules can go through are located in the *x* and *y* axes, but there are secondary channels in the *z*-axis. The gate to enter these channels is a 8-member ring window with a limiting diameter of 4.0 Å. Therefore, the access is blocked for sulfur hexafluoride while nitrogen can go inside this channels being the interaction molecule-zeolite stronger than in the main channels (Fig. S6 in the ESI). We observe the same behavior in AFY zeolite. This structure consists of a main wide channel along the *z*-axis (6.1 Å) that is interconnected by secondary narrow channels along the other two axes trough 8-menber ring opening windows with a limiting diameter of 4 Å where only nitrogen can fit (Figure S7. In the ESI). Suitable blocks were applied in our simulations to avoid the access of molecules to parts of the structures where they are unable to enter experimentally.

The structures in which the interaction of sulfur hexafluoride with the zeolite is more than two and a half times stronger than the interaction of nitrogen with the zeolite are highlighted as good candidates for the separation process regarding adsorption properties at low loading. These structures are: ASV, FER, ITR, IWW, MWW, KFI, BEC, and SFG. In further discussion we also take into account diffusion and adsorption properties at medium and high coverage and we will compare our findings with these preliminary results.

It is well known that molecular transport inside the pores plays a key role in many applications of nanoporous materials and synergies between molecular adsorption and diffusion in zeolites for separation processes has been established using both simulations and experiments[61]. Some zeolites considered as good candidates based on their adsorption properties could be further discarded due to a poor diffusion of the molecules. Therefore we carried out additional MD simulations to analyze the mean square displacement (MSD) of sulfur hexafluoride (the bulkiest molecule under study) in each zeolite at low loading (2 molecules per simulation cell). Fig. 6 shows the MSD obtained in ASV, BEC, FER, and ITR zeolites. For ASV and FER, the slope of the MSD at long times, where the molecules reach the diffusional regime, is almost flat, meaning that sulfur

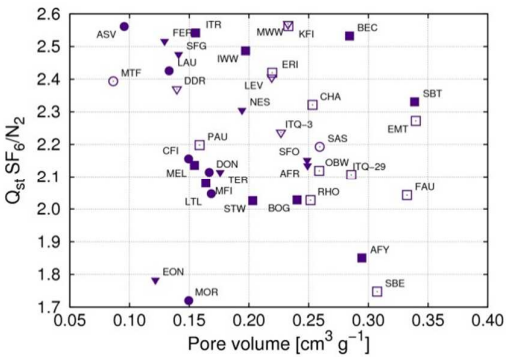

Fig. 5 Ratio of the isosteric heats of adsorption of sulfur hexafluoride and nitrogen at 298 K as a function of the pore volume of the structures. Open symbols show the results obtained for channel-type zeolites and closed symbol for the interconnected-type zeolites. The directionally of the pore space is represented by circles (1D), down triangles (2D), and squares (3D).

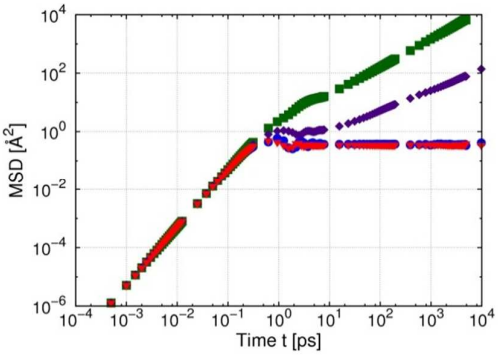

Fig. 6 Mean Square Displacement (MSD) of sulfur hexafluoride in ASV (blue circles), FER (red down triangles), BEC (green squares), and ITR (purple diamonds) zeolites. Simulations were computed at room temperature with two molecules per simulation cell.

hexafluoride diffusion is not allowed in these zeolites. Consequently, we discarded these structures despite the fact that they showed high values of heat of adsorption for sulfur hexafluoride. BEC and ITR were also pointed out as good candidates for the separation process based on the computed heats of adsorption. Fig. 6 shows a non-flat slope from MSD of sulfur hexafluoride in these two zeolites implying that the diffusion of sulfur hexafluoride is permitted in their 3D system. Self-diffusion coefficients for all the zeolites are included in Table S2 in the ESI.

The final set of available zeolites after discarding these in which diffusion of SF_6 is inhibited is: AFR, AFY, BEC, BOG, CFI, DON, EMT, EON, FAU, ITR, IWW, LTL, MEL, MFI, MOR, NES, OBW, SBE, SBT, SFG, SFO, STW, and TER. We computed adsorption isotherms in these structures for binary mixtures containing sulfur hexafluoride (10%) and nitrogen (90%) at room temperature. Fig. 7 shows the adsorption isotherms of the mixture classified in four groups according to the general trend of adsorption.

Fig. 7a shows the values obtained for AFY, EON, MOR, OBW, and STW. In these zeolites the adsorption of sulfur hexafluoride starts at 10 kPa, almost simultaneously than nitrogen adsorption. However loadings of sulfur hexafluoride are larger up to 10^3 kPa. At higher values of pressure we observe a rise on the adsorption of nitrogen that keeps the loading of sulfur hexafluoride almost independent of pressure. The effect is less visible in AFY because this zeolite has the largest pore volume of this group and the competition for available space in the zeolite is not so strong. We already pointed out AFY, EON, and MOR as poor candidates for the separation processes based on the heats of adsorption and due to the existence of sites and channels only accessible for small molecules. These sites or channels allow nitrogen to be adsorbed at low pressure (10 kPa) without competition with sulfur hexafluoride. Furthermore, at higher pressure nitrogen is also able to compete and even displace sulfur hexafluoride from the accessible pore volume for both molecules. In this group of zeolites we found saturation loadings of 0.5-2 mol/kg for sulfur hexafluoride, but the selectivity is expected to be low since the loading of nitrogen is similar or larger than the loading for sulfur hexafluoride at high pressure.

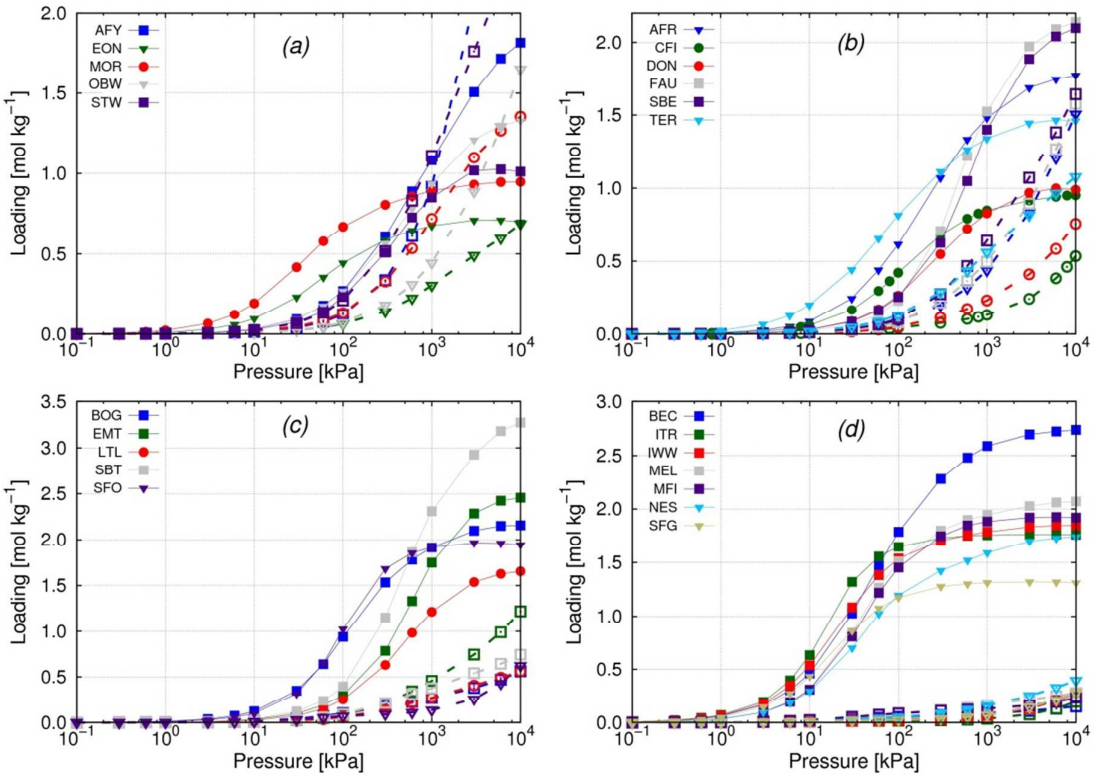

Fig. 7 Computed adsorption isotherms from the binary mixture SF_6/N_2 (0.1:0.9) at room temperature in a) AFY, EON, MOR, OBW, and STW; b) AFR, CFI, DON, FAU, SBE, and TER; c) BOG, EMT, LTL, SBT, and SFO; and d) BEC, ITR, IWW, MEL, MFI, NES, and SFG zeolites. Isotherms of SF_6 are depicted with full symbols and lines and these of N_2 with empty symbols and dotted lines. The directionally of the pore space is represented by circles (1D), down triangles (2D), and squares (3D).

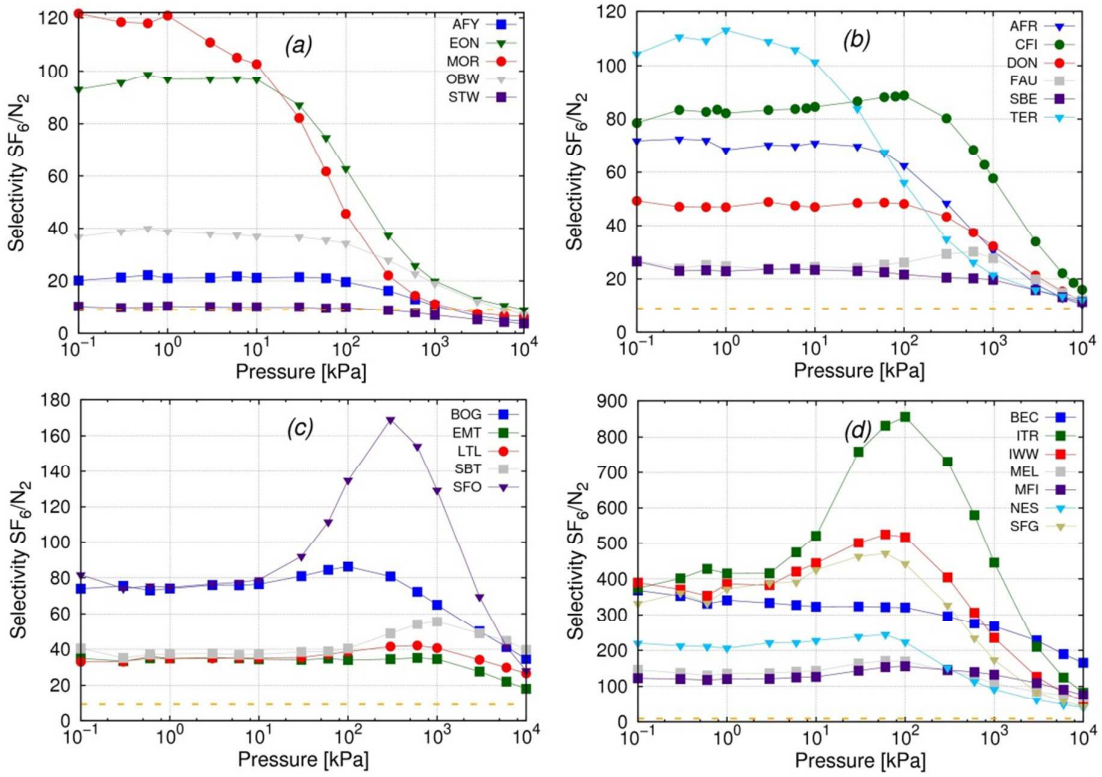

Fig. 8 Adsorption selectivity SF6/N2 from the binary mixture SF6/N2 (0.1:0.9) at room temperature in a) AFY, EON, MOR, OBW, and STW; b) AFR, CFI, DON, FAU, SBE, and TER; c) BOG, EMT, LTL, SBT, and SFO; and d) BEC, ITR, IWW, MEL, MFI, NES, and SFG zeolites. The directionally of the pore space is represented by circles (1D), down triangles (2D), and squares (3D). The inversion in the selective behavior is represented with an orange dotted line.

In Fig. 7b we depict the adsorption isotherms obtained for AFR, CFI, DON, FAU, SBE, and TER zeolites. The adsorption of sulfur hexafluoride starts between 10 and 10^2 kPa, while nitrogen enters the structures at 10^2 kPa. Above 10^3 kPa we observe a displacement of the molecules of SF_6 by the molecules of nitrogen, but the loading of sulfur hexafluoride remains about 0.5 mol/kg higher than the loading of nitrogen at 10^4 kPa. The isotherms calculated for BOG, EMT, LTL, SBT, and SBO zeolites are shown in Fig. 7c. The adsorption performance of sulfur hexafluoride in this group of zeolites is similar than the observed in Fig. 7b, but the adsorption of adsorption nitrogen is now lower. Therefore, loadings of both molecules at the highest pressure of study (10^4 kPa) differ in about 1-2 mol/kg. We found saturation loadings for sulfur hexafluoride between 1-2 mol/kg (Fig. 7b) and 1.5-3.5 mol/kg (Fig. 7c) and selectivity in favor of this molecule is expected to be larger in the latter group.

The isotherms from the last group of zeolites are depicted in Fig. 7d (BEC, ITR, IWW, MEL, MFI, NES, and SFG). The main characteristic of this group is the very low adsorption of nitrogen in the range of pressure under study (10^{-1}-10^4 kPa). Sulfur hexafluoride enters the structures at 1 kPa. At this value of pressure the adsorption of nitrogen is lower than 0.5 kg/mol in all zeolites. Therefore zeolites of this group could be good candidates for selective capture of sulfur hexafluoride, as we pointed out before based on heat of adsorption for ITR, IWW, BEC y SFG.

For a deeper understanding of the selective behavior of the studied zeolites we calculated adsorption selectivities of SF_6 over N_2 according to the expression $(x_{SF6}/y_{N2})/(x_{N2}/y_{SF6})$, where x is the molar fraction in the adsorbed phase and y the molar fraction in the bulk phase. Fig. 8 shows these values of selectivity obtained from the mixture (0.1:0.9) at room temperature in a range of pressure that spans from 0.1 to 10^4 kPa. As a general rule, selectivity remains constant up to 10 kPa, where the loadings of both molecules are still very low. Above 10 kPa, the slope of the selectivity is still flat in most zeolites and only increases for SFO, ITR, IWW and SFG whereas at high (10^2-10^3 kPa) pressure the adsorption of nitrogen reduces the selectivity at high pressure

Using the same classification that we made for adsorption isotherms, zeolites showed in Fig. 8a exhibit the lowest selectivities. EON and MOR have high selectivity at low pressure, but the loading of sulfur hexafluoride is almost negligible (less than 0.25 mol/kg at 10 kPa). The selectivity drops drastically after this pressure, where the adsorption of sulfur hexafluoride is still very low. Increasing pressure up to 10^3 kPa the loading of sulfur hexafluoride in these zeolites reach about 1 mol/kg but at this pressure they do not show preferential adsorption for sulfur hexafluoride. In Fig. 8b the selectivity in favor of sulfur hexafluoride is constant up to 10^2-10^3 kPa but with larger values than these depicted in Fig. 8a as a result of the lower adsorption of nitrogen. As occurs in previous figure, at the highest pressure the selectivity is

reduced due to the displacement of the molecules of SF_6 by these of N_2.

In Fig. 8c there are two zeolites (BOG and SFO) exhibiting twice the selectivity than the rest of the group in the range of pressure that spans from 10 to 10^2 kPa. Above the latter value of pressure the selectivity in SFO increases again and then drops (at 300 kPa) with more than 1.5 mol/kg for SF_6 while nitrogen requires higher pressure to enter the zeolite. Finally the low adsorption of nitrogen showed for zeolites depicted in Fig. 7d (less than 0.5 kg/mol) makes of these structures the best candidates to achieve the largest selectivities in favor of sulfur hexafluoride (Fig. 8d).

As can be seen in Fig. 8, the largest selectivity in favor of sulfur hexafluoride is obtained at 10^2-10^3 kPa. Therefore in Fig. 9 we depict the selectivity obtained for the zeolites at $3{\cdot}10^2$ kPa as a function of (a) zeolite pore volume, and (b) loading of sulfur hexafluoride. We selected this pressure using criteria that combines both high selectivity and loading of the molecule of interest (SF_6). As an exception, we focused on $3{\cdot}10^3$ kPa for EMT, LTL, SBT, FAU, and SBE and $3\text{-}6{\cdot}10^1$ kPa for TER, EON, and MOR (see Table S3 in the ESI). The zeolite with the largest selectivity in favor of sulfur hexafluoride is ITR, followed by IWW, SFG and BEC. The high selectivity of this structure can be attributed to the topology. ITR consists on straight channels along the *x*-axe interconnected by zig-zag channels. The size of these channels (5.12 Å) is very close to the kinetic diameter of SF_6 and therefore this molecule is commensurate with the pore leading to saturation at 10^2 kPa when nitrogen is not yet adsorbed. A similar explanation could be used for SFG, but its lower pore volume makes lower the saturation loading of SF_6 and consequently its selectivity. The adsorption of SF_6 in these zeolites is about 1-2.5 mol/kg, being BEC the zeolite with the largest saturation capacity in this group. This is due to the high pore volume that makes of this zeolite the best candidate for storage. SBT zeolite could also be used in a second stage as storage material with a pore volume 0.35 cm^3/g, but its selectivity is very low compared to the other remarked zeolites.

Although to find a relationship between the framework topology of the zeolites and the selectivity of sulfur hexafluoride is not straight forward, we observed that the separation of the mixture SF_6/N_2 is more efficient using zeolites with intersecting channels accessible to the two molecules. These accessible channels should cross forming intersections of a minimum of 6.3 and a maximum of 7.1 Armstrong in diameter. These patterns were exhibited by the 2-dimension structures ITR and SFG and the 3-dimension structures BEC and IWW.

Conclusions

We used molecular simulations to evaluate the suitability of zeolites as molecular sieves to separate sulfur hexafluoride from nitrogen. The prediction of zeolites for this separation

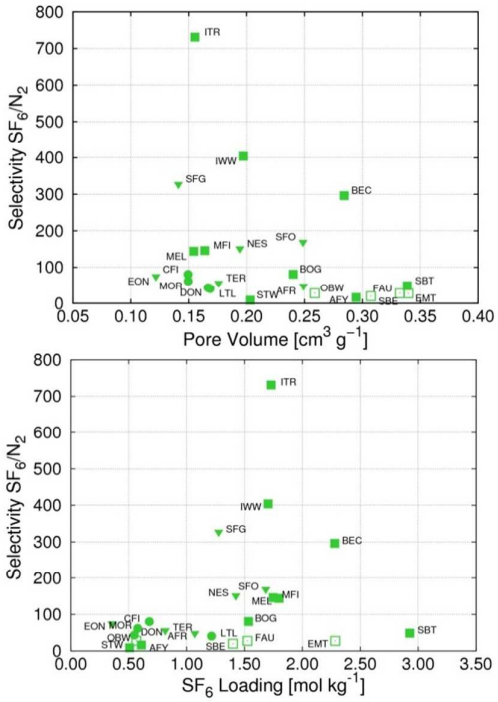

Fig. 9 Adsorption selectivity SF_6/N_2 from the binary mixture SF_6/N_2 (0.1:0.9) at room temperature as function of (a) zeolite pore volume and (b) loading of sulfur hexafluoride. Open symbols show the results obtained for channel-type zeolites and closed symbol this for interconnected-type, being the directionally of the pore space represented by circles (1D), down triangles (2D), and squares (3D). Selectivity is calculated at the pressure with higher selectivity and loading of SF_6 for each structure.

was based on the adsorption and diffusion performance. At low loading the largest molecule, i.e. sulfur hexafluoride, exhibits the strongest interaction with all selected zeolites. The adsorption of nitrogen increases with the pressure being the $3{\cdot}10^2$-$3{\cdot}10^3$ kPa the best range for selective adsorption of sulfur hexafluoride over nitrogen. At these values of pressure sulfur hexafluoride is reaching saturation while nitrogen is starting to be adsorbed. Isosteric heats of adsorption confirm the preferential adsorption of sulfur hexafluoride at low loading. Our results show that local structure features dominate the strength of adsorption in zeolites such as MOR, EON, SBE, and AFY, providing exclusive adsorption sites for nitrogen that reduce the affinity for sulfur hexafluoride. Therefore, the selectivity over sulfur hexafluoride in these structures is the lowest of the studied zeolites. Based only on the heats of adsorption we pointed out zeolites ASV, FER, ITR, IWW, MWW, KFI, BEC, and SFG as good candidates for the separation processes. However, zeolites ASV, FER, MWW, and KFI were discarded due to the slow diffusion of sulfur hexafluoride in their pores. Based on the combination of good performance on adsorption and diffusion we point out zeolites BEC, ITR, IWW, and SFG as the most efficient candidates for the selective capture of sulfur hexafluoride form this particular mixture.

Acknowledgements

This work was supported by the European Research Council through an ERC Starting Grant (ERC2011-StG-279520-RASPA), by the MINECO (CTQ2013-48396-P) and by the Andalucía Region (FQM-1851). I. Matito-Martos and A. Martín-Calvo thank the Spanish "Ministerio de Educación Cultura y Deporte" for their predoctoral fellowships.

Notes and references

1. L. G. Christophorou and R. J. Van Brunt, *Dielectrics and Electrical Insulation, IEEE Transactions on*, 1995, **2**, 952-1003.
2. S. Builes, T. Roussel and L. F. Vega, *AIChE Journal*, 2011, **57**, 962-974.
3. F. De Alba, *JAMA*, 2010, **303**, 1204-1204.
4. N. Lassau, L. Chami, B. Benatsou, P. Peronneau and A. Roche, *European radiology* 2007, **17 Suppl 6**, 89-98.
5. J. Zhang, J. Z. Zhou, Q. Liu, G. R. Qian and Z. P. Xu, *Environmental Science & Technology*, 2013, **47**, 6493-6499.
6. M. Rigby, J. Muehle, B. R. Miller, R. G. Prinn, P. B. Krummel, L. P. Steele, P. J. Fraser, P. K. Salameh, C. M. Harth, R. F. Weiss, B. R. Greally, S. O'Doherty, P. G. Simmonds, M. K. Vollmer, S. Reimann, J. Kim, K. R. Kim, H. J. Wang, J. G. J. Olivier, E. J. Dlugokencky, G. S. Dutton, B. D. Hall and J. W. Elkins, *Atmospheric Chemistry and Physics*, 2010, **10**, 10305-10320.
7. I. Cha, S. Lee, J. D. Lee, G.-W. Lee and Y. Seo, *Environmental Science & Technology*, 2010, **44**, 6117-6122.
8. Houghton J. T., Meira Filho L. G., Callander B. A., Harris N., Kattenberg A. and Maskell K., Cambridge, U. K., 1996.
9. M. Maiss and C. A. M. Brenninkmeijer, *Environmental Science & Technology*, 1998, **32**, 3077-3086.
10. C.-H. Tsai and J.-M. Shao, *Journal of Hazardous Materials*, 2008, **157**, 201-206.
11. M. Radoiu and S. Hussain, *Journal of Hazardous Materials*, 2009, **164**, 39-45.
12. X. Song, X. Liu, Z. Ye, J. He, R. Zhang and H. Hou, *Journal of Hazardous Materials*, 2009, **168**, 493-500.
13. Y. Yamada, H. Tamura and D. Takeda, *The Journal of Chemical Physics*, 2011, **134**, 104302.
14. L. G. Christophorou;, J. K. Olthoff; and D. S. Green;, *Gases for Electrical Insulation and Arc Interruption: Possible Present and Future Alternatives to Pure SF6*, Boulder, CO, NIST Tech. Note 1425, 1997.
15. M. Toyoda, H. Murase, T. Imai, H. Naotsuka, A. Kobayashi, K. Takano and K. Ohkuma, *Power Delivery, IEEE Transactions on*, 2003, **18**, 442-448.
16. O. Yamamoto, T. Takuma and M. Kinouchi, *Electrical Insulation Magazine, IEEE*, 2002, **18**, 32-37.
17. H. Hama, M. Yoshimura, K. Inami and S. Hamano, in *Gaseous Dielectrics VIII*, eds. L. Christophorou and J. Olthoff, Springer US, 1998, DOI: 10.1007/978-1-4615-4899-7_48, ch. 48, pp. 353-359.
18. K. Inami, Y. Maeda, Y. Habuchi, M. Yoshimura, S. Hamano and H. Hama, *Electrical Engineering in Japan*, 2001, **137**, 25-31.
19. M. S. Sun, D. B. Shah, H. H. Xu and O. Talu, *The Journal of Physical Chemistry B*, 1998, **102**, 1466-1473.
20. D. V. Cao and S. Sircar, *Adsorption*, 2001, **7**, 73-80.
21. I. Senkovska, E. Barea, J. A. R. Navarro and S. Kaskel, *Microporous and Mesoporous Materials*, 2012, **156**, 115-120.
22. P. Chowdhury, C. Bikkina and S. Gumma, *The Journal of Physical Chemistry C*, 2009, **113**, 6616-6621.
23. P. Chowdhury, C. Bikkina, D. Meister, F. Dreisbach and S. Gumma, *Microporous and Mesoporous Materials*, 2009, **117**, 406-413.
24. Y. C. Chiang and P. Y. Wu, *Journal of Hazardous Materials*, 2010, **178**, 729-738.
25. S. Furmaniak, A. P. Terzyk, P. A. Gauden and P. Kowalczyk, *Microporous and Mesoporous Materials*, 2012, **154**, 51-55.
26. J. Jagiełło, T. J. Bandosz and J. A. Schwarz, *Langmuir*, 1997, **13**, 1010-1015.
27. T. J. Bandosz, J. Jagiełło and J. A. Schwarz, *Journal of Chemical & Engineering Data*, 1996, **41**, 880-884.
28. S. Himeno, T. Tomita, K. Suzuki, K. Nakayama, K. Yajima and S. Yoshida, *Industrial & Engineering Chemistry Research*, 2007, **46**, 6989-6997.
29. E. Garcia-Perez, J. B. Parra, C. O. Ania, A. Garcia-Sanchez, J. M. Van Baten, R. Krishna, D. Dubbeldam and S. Calero, *Adsorpt.-J. Int. Adsorpt. Soc.*, 2007, **13**, 469-476.
30. M. D. Romero, G. Ovejero, A. Rodríguez and J. M. Gómez, *Microporous and Mesoporous Materials*, 2005, **81**, 313-320.
31. G. N. Altshuler and G. Y. Shkurenko, *Bulletin of the Academy of Sciences of the USSR Division of Chemical Science*, 1990, **39**, 1331.
32. J. P. Anerousis, *Chemical Engineering*, 1976, **83**, 128.
33. I. Matito-Martos, A. Martin-Calvo, J. J. Gutierrez-Sevillano, M. Haranczyk, M. Doblare, J. B. Parra, C. O. Ania and S. Calero, *Physical Chemistry Chemical Physics*, 2014, **16**, 19884-19893.
34. M. P. Bernal, J. Coronas, M. Menendez and J. Santamaria, *Aiche Journal*, 2004, **50**, 127-135.
35. S. Calero, A. Martin-Calvo, S. Hamad and E. Garcia-Perez, *Chem. Commun.*, 2011, **47**, 508-510.
36. A. Martin-Calvo, E. Garcia-Perez, A. Garcia-Sanchez, R. Bueno-Perez, S. Hamad and S. Calero, *Physical Chemistry Chemical Physics*, 2011, **13**, 11165-11174.
37. National Institute of Standards and Technology, http://www.nist.gov/index.html, (accessed January, 2013).
38. M. P. Allen; and D. J. Tildesley, *Computer Simulation of Liquids*, Oxford Clarendon Press, 1987.
39. C. Baerlocher, L. B. McCusker and D. H. Olson, *Atlas of Zeolite Framework types*, Elsevier, London, Sixth edn., 2007.
40. A. Garcia-Sanchez, D. Dubbeldam and S. Calero, *Journal of Physical Chemistry C*, 2010, **114**, 15068-15074.
41. A. Martin-Calvo, J. J. Gutierrez-Sevillano, J. B. Parra, C. O. Ania and S. Calero, *The Journal of Physical Chemistry C*, 2015, **Submitted**.

42. A. Garcia-Sanchez, C. O. Ania, J. B. Parra, D. Dubbeldam, T. J. H. Vlugt, R. Krishna and S. Calero, *Journal of Physical Chemistry C*, 2009, **113**, 8814-8820.
43. D. Dubbeldam, S. Calero, E. Donald and R. Snurr, *Molecular Simulation*, 2015, **10.1080/08927022.2015.1010082**.
44. D. Frenkel and B. Smit, *Understanding Molecular Simulations: From Algorithms to Applications; second edition ed.*, 2002.
45. T. Duren, L. Sarkisov, O. M. Yaghi and R. Q. Snurr, *Langmuir*, 2004, **20**, 2683-2689.
46. S. Calero, D. Dubbeldam, R. Krishna, B. Smit, T. J. H. Vlugt, J. F. M. Denayer, J. A. Martens and T. L. M. Maesen, *Journal of the American Chemical Society*, 2004, **126**, 11377-11386.
47. R. Krishna and J. M. van Baten, *Langmuir*, 2010, **26**, 2975-2978.
48. J. Kim, R. L. Martin, O. Rubel, M. Haranczyk and B. Smit, *J. Chem. Theory Comput.*, 2012, **8**, 1684-1693.
49. A. Martin-Calvo, F. D. Lahoz-Martin and S. Calero, *Journal of Physical Chemistry C*, 2012, **116**, 6655-6663.
50. G. S. Pawley, *Mol. Phys.*, 1981, **43**, 1321-1330.
51. P. K. Ghorai and S. Yashonath, *J. Chem. Phys.*, 2004, **120**, 5315-5321.
52. D. Dellis and J. Samios, *Fluid Phase Equilibria*, 2010, **291**, 81-89.
53. J. S. Rowlinson and F. L. Swinton, *Liquids and Liquid Mixtures*, Butterworths, London, 1982.
54. J. S. Rowlinson and B. Widom, *Molecular Theory of Capillarity*, Oxford University Press, New Yoek, 1989.
55. P. W. Atkins, *Physical Chemistry*, Oxford Higher Education, New York, 1990.
56. M. G. Martin and J. I. Siepmann, *The Journal of Physical Chemistry B*, 1998, **102**, 2569-2577.
57. J. A. Dunne, R. Mariwals, M. Rao, S. Sircar, R. J. Gorte and A. L. Myers, *Langmuir*, 1996, **12**, 5888-5895.
58. M. S. Sun, D. B. Shah, H. H. Xu and O. Talu, *Journal of physical chemistry B*, 1998, **102**, 1466-1473.
59. H. MacDougall, D. M. Ruthven and S. Brandani, *Adsorption-Journal of the International Adsorption Society*, 1999, **5**, 369-372.
60. R. L. Martin, T. F. Willems, L. C. Lin, J. Kim, J. A. Swisher, B. Smit and M. Haranczyk, *ChemPhysChem*, 2012, **13**, 3595-3597.
61. T. Titze, C. Chmelik, J. Kärger, J. M. van Baten and R. Krishna, *The Journal of Physical Chemistry C*, 2014, **118**, 2660-2665.